Article

Synthesis, Single Crystal X-Ray Structure, Theoretical Studies of Triple-{Mn^{III}-Schiff-Base}-Decorated Molybdate

Jian-Chang Xiao [1,†], **Qiong Wu** [1,2,*,†] 📷, **Yuan Lei** [1], **Jin-Rong Sun** [1], **Fang Jiang** [1], **Yan Xu** [1], **Xin-Di Xu** [1] **and Tianyu Li** [1]

1   Department of Chemistry and Chemical Engineering, Kunming University, Kunming 650214, China; xiaojianchangkm@sina.com (J.-C.X.); ly1393579096@hotmail.com (Y.L.); sjr15887410670@hotmail.com (J.-R.S.); f2106578268@hotmail.com (F.J.); xy23016942771@hotmail.com (Y.X.); xu1768644060@sohu.com (X.-D.X.); ltyytl999@sina.com (T.L.)
2   Yunnan Provincial Research Center for Plastic Films Engineering Technology, Kunming 650214, China
*   Correspondence: wuqiongkm@sina.com
†   These authors contribute equally to this work.

Abstract: The design and synthesis of magnets with low dimensionality is currently an attractive research topic. The reaction of a Schiff base metal complex with simple molybdate has led to the formation of a new {Mn^{III}-Schiff-base}-decorated molybdate heterometallic cluster, [{Mn(salpn)(H$_2$O)}$_3$MoO$_4$] (CH$_3$COO)·2H$_2$O (**1**) (salpn = *N,N'*-(1,3-propylene)bis(salicylideneiminate)). The hybrid aggregate was characterized using a range of methods including elemental analysis, single crystal x-ray diffraction, Infrared spectra (IR) spectroscopy, and x-ray structural analysis. The crystals of **1** are hexagonal: *P6$_3$/m*, a = 14.027(5) Å, c = 17.487(5) Å, *V* = 1142.6(3) Å^3. Structural analyses indicate that we report on the preparation of the first triple metallic-oligomer held by orthomolybdate. Density functional theoretical calculation (DFT) studies have been performed to calculate electronic structure and potential energy landscapes. Additionally, the magnetic property of **1** indicates an antiferromagnetic coupling between the metal centers in the complex.

Keywords: Schiff base; heterometallic cluster; density functional theory; magnetic behavior

1. Introduction

Organic-inorganic hybrids, a class of promising materials that simultaneously combine the remarkable features of both components into one material, presenting properties from either part of the distinctive building blocks, have become a focus of research interest in the past few decades [1–4]. In recent years, more and more attention has been paid to Schiff base hybrids, not only because of their variety of architectures and fascinating topologies, but also for their remarkable applications in magnetism, asymmetric catalysis, adsorption, and medicine [5–8]. Thanks to the higher thermal and chemical stability of inorganic carriers, the migration of metal Schiff base building blocks onto inorganic carriers conceives an alternative scientific method for the construction of new types of hybrid materials [9,10].

In recent years, various types of pure inorganic building blocks have been successfully introduced into Mn-salen molecular packing in crystals. This opens up a plethora of applications ranging from the synthesis of interesting magnetic compounds to the explorations of magnetic exchange [11–15]. As reported by our group previously, the introduction of diamagnetic B-type Anderson polyoxometalates (POMs) into Mn-dimer Schiff base precursors has led to the extraction of their intrinsic SMM

behavior [16]. In the next couple of years, the continuous quest for large-size inorganic building units, especially the classical saturated polyoxoanion, incorporated with Mn^{III} (Schiff base) systems will yield a sequence of new magnetic hybrids [17–20]. Although a vast number of saturated or monovacant polyoxoanions are known as a unique class of building units from which Mn-salen compounds are derived, tiny inorganic moieties largely remain unexplored. Meanwhile, the mechanism of the formation of crystalline materials has not been well clarified, especially for hybrid species compounds. Therefore, whether in theory or in practice, it is vital in the search for new reactions, which will in turn aid the investigation into the relationship between the hybrid structure and diverse precursors derived from the well-characterized Mn-Schiff based family and different inorganic building blocks.

Based on the above considerations, we introduce the molybdate $(NH_4)_6Mo_7O_{24} \cdot 4H_2O$ and $[Mn(salpn)(H_2O)]^+$ as starting materials for our design strategy resulting in the formation of a supramolecular aggregate $[\{Mn(salpn)(H_2O)\}_3MoO_4](CH_3COO) \cdot 2H_2O$ (**1**) (salpn = *N,N′*-(1,3-propylene)bis(salicylideneiminate)), see Scheme 1). As far as we know, compound **1** represents the first example of a triple metallic-oligomer linked by orthomolybdate.
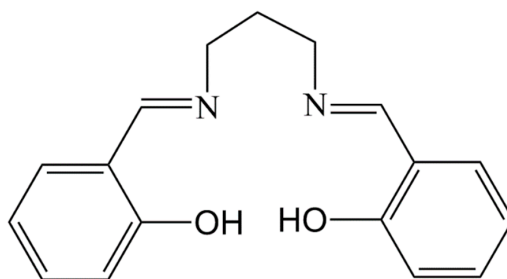
Scheme 1. Molecular structure of title compound.

2. Experimental

2.1. General

All chemicals and solvents were commercially purchased and used as received (Aladdin, Shanghai, China). C, H, N, Mn, and Mo elemental analyses were performed on a Perkin-Elmer 240C atomic absorption spectrophotometer and a PLASMA-SPEC(1) ICP atomic emission spectrometer (PerkinElmer, Shanghai, China), respectively. IR spectra (Bruker, Karlsruhe, Germany) in 4000–400 cm^{-1} were measured with an Alpha-Centauri spectrometer from KBr pellets. $[Mn(salpn)(H_2O)]_2(CH_3COO)_2$ was prepared using a scaled-down version of Wei's 1999 procedure [21].

Magnetic susceptibility measurements were carried out with powdered sample (16.52 mg) of the title compound using a Quantum Design SQUID-MPMS magnetometer (Quantum Design, San Diego, CA, USA). Diamagnetic corrections were made with Pascal's constants for all the manganese atoms [22].

2.2. Synthesis

$[Mn(salpn)(H_2O)]_2(CH_3COO)_2$ (0.79 g) was dissolved in a methanol/water mixed solvent (15 mL). The solution was then stirred vigorously in a 100 mL Erlenmeyer flask to achieve a uniform mixture. Then, $(NH_4)_6Mo_7O_{24} \cdot 4H_2O$ (20 mL, 0.247 g) (Aladdin, Shanghai, China) was added to the mixture, and the pH was adjusted to 3.5. The solution was heated to 40 °C, stirred for another 3 h, and the resulting clear dark brown solution was filtered at room temperature, then the filtrate was left undisturbed in a flask sealed with pierced parafilm (Solarbio, Oshkosh, Wisconsin, USA). Brown crystals of **1** were isolated after one week. The hexagonal crystals were collected by filtration, washed with methanol, and dried under inert atmosphere. Yield: 31% based on Mo. Elemental analysis, calcd: $C_{53}H_{55}Mn_3MoN_6O_{17}$ **1**: C, 48.63; H, 4.23; N, 6.42; Mn, 12.59; Mo, 7.33%; Found: C, 48.41; H, 4.20; N, 6.51; Mn, 12.61; Mo, 7.35 %. IR (KBr pellet, cm^{-1}): 3376(m), 1612(s), 1542(s), 1451(s), 1395(m), 1271(s), 1119(m), 985(w), 904(s), 813(w), 771(w).

2.3. Crystal Structure Determination

Single crystal x-ray diffraction data were recorded on a Rigaku R-AXIS RAPID (Rigaku, Tokyo, Japan) image plate diffractometer (Mo KR radiation, λ = 0.71073 Å, room temperature). The total number of reflections measured was 21,315 (1822 unique, R_{int} = 0.0425). The heavy atoms were positioned with Patterson methods, while the remaining atoms were found using Fourier techniques. The structures were refined with the Olex2 refinement package using a full-matrix least-squares with respect to F^2 [23]. Due to the presence of highly disordered solvent molecules and counter ions, the dataset was treated with the SQUEEZE [24] routine of the PLATON software [25] suite used to remove the contribution of the highly disordered lattice guests, and one counter ion acetate anion as well as two water molecules were estimated from the results of SQUEEZE and elemental analysis, where the assessment method and result are in accordance with a previously reported penta-nuclear analogue [13]. In the refinement process, the non-hydrogen atoms were refined anisotropically. The hydrogen atoms were geometrically located at calculated positions and refined in the riding model. As for the –CH$_2$- structure, the refinement procedure obtained C–H = 0.97 Å, U_{iso} (H) = 1.5 U_{eq} of the attached C atoms for coordinated water molecules and 1.2 U_{eq}(C) for other H atoms, and aromatic C–H = 0.93Å. The crystallographic data and refinement parameters are given in Tables 1, S1 and S2 (Supplementary Materials).

Table 1. Crystallographic characteristics of the compounds and parameters of the diffraction experiment.

| Parameter	Value I
Formula	$C_{53}H_{55}Mn_3MoN_6O_{17}$
Mr (g mol^{-1})	1326.89
Temperature/K	293(2)
Wavelength/Å	0.71073
Crystal system	hexagonal
space group	$P6_3/m$
a/Å	14.027(5)
b/Å	14.027(5)
c/Å	17.487(5)
Volume/Å^3	1142.6(3)
Z	0.16667
Calculated density	1.442 Mg/m^3
Absorption coefficient	0.896 mm^{-1}
F(000)	1320
Theta range for data collection	3.13 to 25.00 deg
Limiting indices	−16 <= h <= 16, −16 <= k <= 16, −20 <= l <= 19
Reflections collected/unique	21,315/1822 [R(int) = 0.0425]
Completeness to theta = 25.00	99.7 %
Refinement method	Full-matrix least-squares on F^2
Goodness-of-fit on F^2	*1.203*
Final R indices [I > 2sigma(I)]	R_1 = 0.0543, wR_2 = 0.1842
R indices (all data)	R_1 = 0.0584, wR_2 = 0.1871
Largest diff. peak and hole, e.Å^{-3}	0.713 and −0.710

CCDC-1948862 contains the crystallographic data. The data can be obtained free of charge by contacting the Cambridge Crystallographic Data Centre, 12 Union Road, Cambridge CB2 IEZ, UK., or via http://www.ccdc.cam.ac. uk/datarequset/cif. Fax: +44(0)-1223-336033 [26].

3. Results and Discussion

3.1. Crystal Structure

As is shown in Figure 1, there is a half Schiff-base ligand, one manganese cation, one molybdenum center with a 50% occupancy rate, and three oxygen atoms in the asymmetric unit, and the entire cationic [{Mn(salpn)(H$_2$O)}$_3$MoO$_4$]$^+$ unit is composed of a [MoO$_4$]$^{2-}$ center and three Mn^{III} salen-type moieties

(Figures 2 and S1 (Supplementary Materials)). The $[MoO_4]^{2-}$ center exhibits a classic tetrahedron orthomolybdate structure in which the Mo^{6+} is tetrahedrally surrounded by four oxygen atoms. Three of these latter act as bridging ligands linked to {Mn(salpn)(H$_2$O)} units (the bridging oxygen atom and the terminal one are O2 and O3, respectively). The center Mo atom is disordered and appears at two positions with identical occupancy in the $[MoO_4]^{2-}$ unit. The Mo(1)–O(2) bond length is of 1.745(5) Å, with the O–Mo–O angle being of ca. 109.68(5)°. As shown by bond valence sum (BVS) calculations [24] and XPS spectroscopy data, the Mo is in the +6 oxidation state (Table 2). Additionally, Mn^{III} ions exhibit the bipyramid coordination mode in the {Mn(salpn)(H$_2$O)}$^+$. [N2O2] atoms from the salpn ligand form the equatorial plane of Mn^{III}. The distance of Mn–O(N) is 1.92(4) Å. The apical positions are occupied by two oxygen atoms from a $[MoO_4]^{2-}$ group and coordination H$_2$O molecule with Mn-O(H$_2$O)/O($[MoO_4]^{2-}$) bond lengths ranging from 2.386(5) to 2.146(5) Å due to the presence of John-Teller distortion. As seen in the BVS calculations [24] and XPS spectra (ESI, Figure S2 (Supplementary Materials)), all Mn centers are in the +3 oxidation state (Table 2).
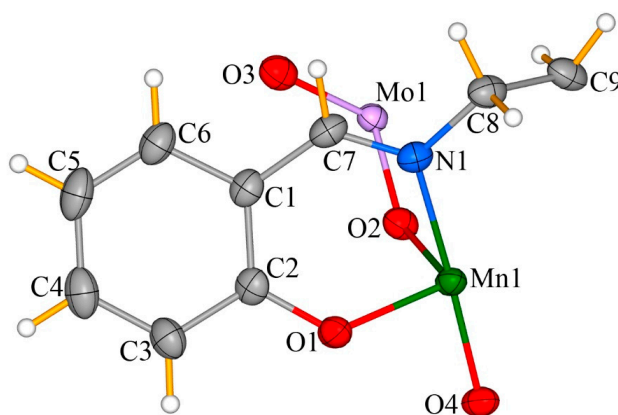

Figure 1. Ball-and-stick and polyhedral illustration of the cationic hybrid cluster [{Mn(salpn)(H$_2$O)}$_3$MoO$_4$]$^+$ cluster of **1**.
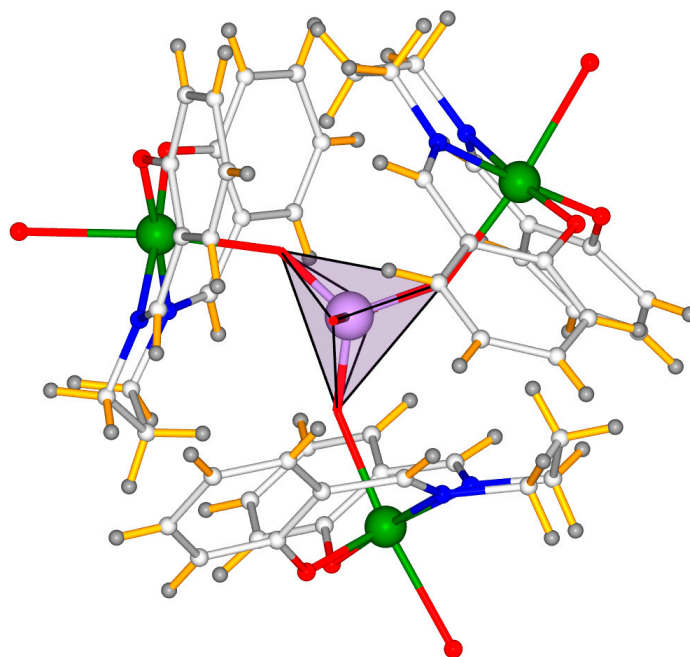
Figure 2. Mixed polyhedral-ball & stick representation of [{Mn(salpn)(H2O)}3MoO4]+ cluster of **1**.

Three {Mn(salpn)(H₂O)} moieties linked to the oxygen atoms of $[MoO_4]^{2-}$ center are assembled in a staggered arrangement, resulting into the cationic cluster with a C_3 symmetry (see Figures 1 and 2). It is worth pointing out that, even though inorganic orthomolybdate/tungstate was proven to have the potential as versatile functional building blocks for the design of heterometallic clusters, up to now, only double and quadruple examples have been documented in the literature [13,14], and no example of triple-metal-organic fragments supported by orthomolybdate has been reported to date. Therefore, to the best of our knowledge, the structure of **1** exhibits the first tetranuclear heterometallic aggregate constructed with orthomolybdate and metal-Schiff base moieties. Moreover, according to the result of PLATON software [25], probability due to the present of counter cation and solvent molecules, the nearest distance between the benzene rings is longer than 4 Å, under this scenario, we deduce that electrostatic attraction and hydrogen bonding are the main driving forces in stabilizing the 3D structure of the title compound. The packing diagram of **1** along three different directions are shown in Figure 3.
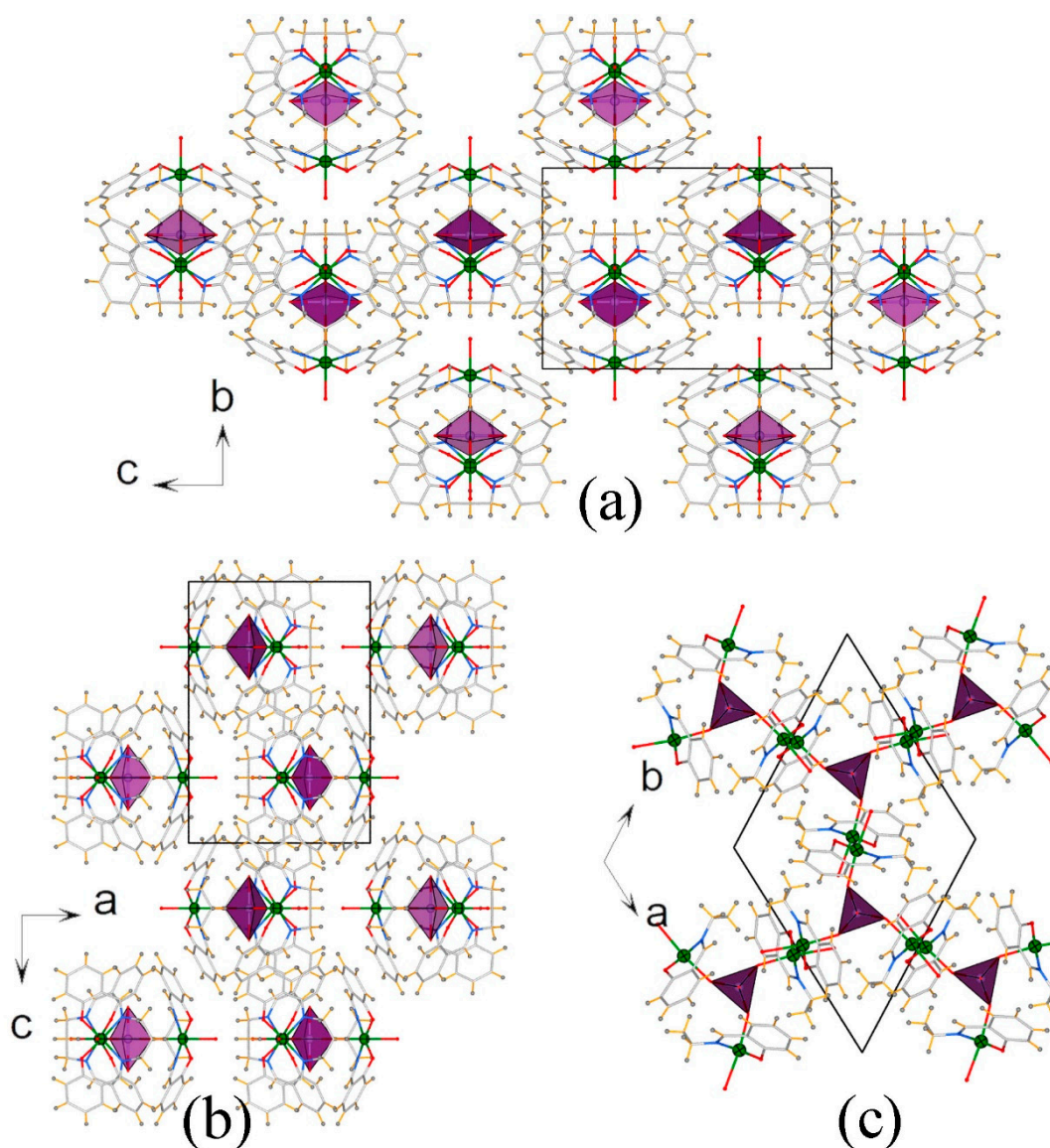
Figure 3. The packing diagrams viewed along the a-axis (**a**), b-axis (**b**), and c-axis (**c**). The compound crystallizes in the hexagonal sp. gr. *P6₃/m*.

Table 2. Bond valence sum calculations of Mn and Mo centers in **1**.

Mn1 2.97 $r_o = 1.76$ Å [a]	**Mo1 6.50 $r_o = 1.907$ Å [a]**
Mn1−O4 1.878 d = 2.147(4)	Mo1−O3 1.856 d = 1.685(13)
Mn1−O4 2.386 d = 1.981(7)	Mo1−O2#2 1.549 d = 1.745(4)
Mn1−N1 2.024 d = 2.020(7)	Mo1−O2#1 1.549 d = 1.745(4)
Mn1−N1#3 2.024 d = 2.043(7)	Mo1−O2#3 1.549 d = 1.745(4)
Mn1−O1 2.146 d = 2.055(7)	
Mn1−O2 2.386 d = 2.067(7)	

Symmetry code: #1 −x + y − 1, −x − 1, −z + 1/2; #2 −y − 1, x − y,z; #3 x,y, −z + 1/2

3.2. Porous Analysis

Furthermore, the heterometallic [{Mn(salpn)(H$_2$O)}$_3$MoO$_4$]$^+$ clusters are linked via hydrogen bonds and intermolecular interactions to assemble into larger structures and the calculated inner surface of the porous framework is shown along with them (Figure 4) [27,28]. The porous between the cationic heterometallic clusters are isolated from each other, and the program PLATON [25] indicates that the potential solvent area has a diameter of about 7 Å and possesses a 474.5 Å^3 void of a total 15.9% space in the unit cell. It is noteworthy that because the SQUEEZE routine [24] was used to remove the highly disordered reflections of the dataset, the calculated empty spaces are probably filled with acetate counter ions and solvent water molecules.
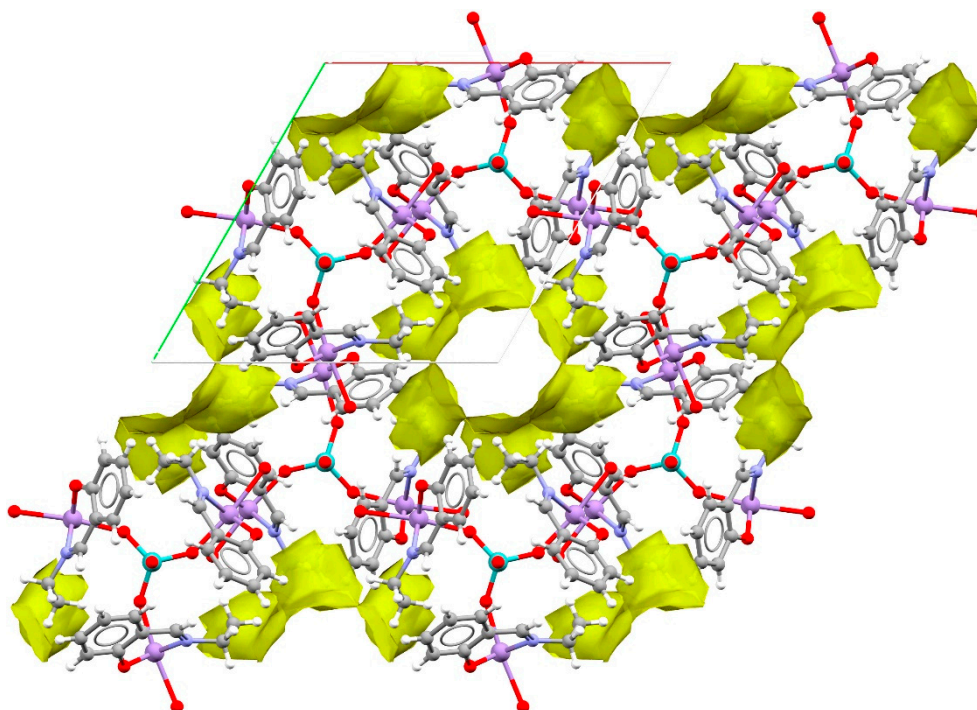
Figure 4. The empty spaces in the packing crystal structure of **1**.

3.3. Frontier Molecular Orbitals

The frontier molecular orbitals (FMO) play a significant role in revealing the electronic properties, the kinetical stability, and chemical reactivity of the complex [29]. DFT calculations were carried out at the B3LYP/6-311+G(d,p) level of theory. The Frontier molecular orbitals 3D plots of 1 are displayed in Figure 5.
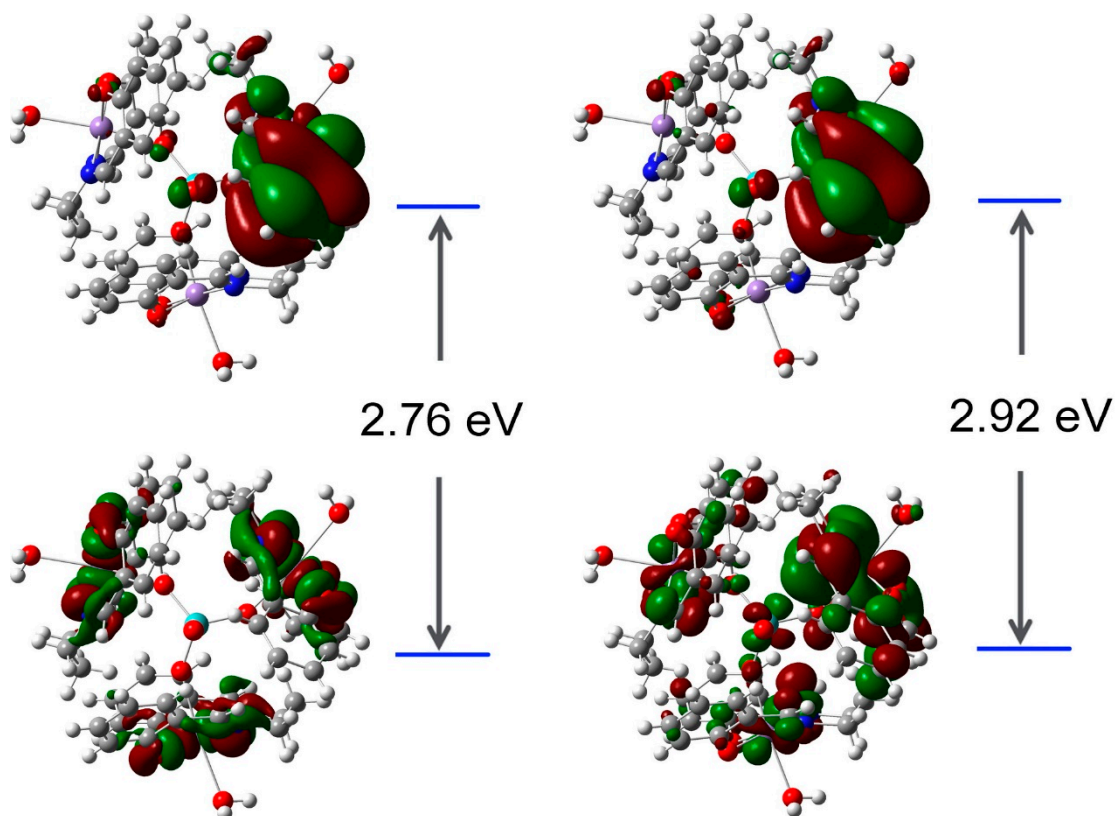
Figure 5. Frontier molecular orbital plots of the title compound obtained by the B3LYP/6-311G (d,p) method.

It was revealed that the HOMO (highest occupied molecular orbital) surfaces are localized mostly over the {Mn(salpn)(H$_2$O)}$^+$cations, whilst the LUMO (lowest unoccupied molecular orbital) surfaces are over the molecule. This suggests that electronic communication exists between [MoO$_4$]$^{2-}$ and metal–organic units. The value of the energy separation between the HOMO and LUMO was also calculated as 3.35 eV for the α orbitals and 3.51 eV for β orbitals, respectively, which indicates a high kinetic stability of **1**.

3.4. Magnetic Properties

Magnetic susceptibility measurements were carried out on the powdered sample of the title compound. Temperature-dependent magnetism susceptibility data were collected over the temperature range of 2 to 300 K with $\chi_m T$ vs T displayed in Figure 6.

The generation of magnetic behavior of **1** from the Mn^{III} ions can be ascribed to the diamagnetic [MoO$_4$]$^{2-}$. The $\chi_m T$ value of **1** decreases slowly with decreasing temperature from 9.1 cm^3·mol^{-1}·K at 300 K to 8.2 cm^3·mol^{-1}·K at 50 K. Upon further cooling, the $\chi_m T$ value drops rapidly to a minimum value of 0.51 cm^3·mol^{-1}·K at 2.0 K.

The $\chi_m T$ value at 300 K is slightly higher than the spin-only value of 9 cm^3·mol^{-1}·K for three uncoupled Mn(III) with S = 4 and g = 2. The χ^{-1} versus T obeys the Curie–Weiss law over the whole temperature range, providing parameters of C = 9.37 cm 3·K·mol^{-1} and θ = −7.41 K. The negative θ values indicate that there exists overall antiferromagnetic behavior of the title compound.
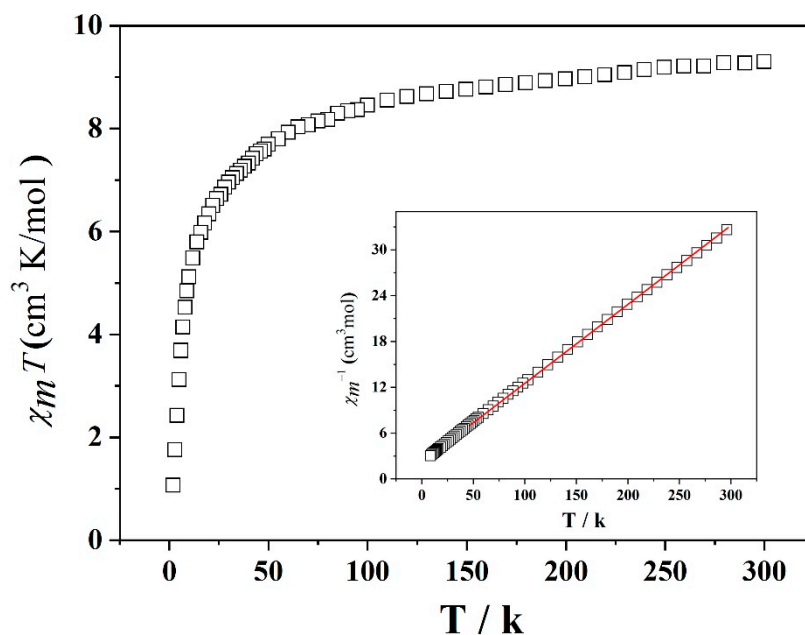
Figure 6. Temperature dependence of $\chi_m T$ vs. T of **1** from 2 to 300 K.

4. Conclusions

In conclusion, we have synthesized and structurally characterized a new organic-inorganic hybrid [{Mn(salpn)(H$_2$O)}$_3$MoO$_4$](CH$_3$COO)·2H$_2$O (**1**) (salpn = *N,N'*-(1,3-propylene)bis(salicylideneiminate)). Structural analyses show that compound **1** represents the first example of tri-metallic-polymer decorated orthomolybdate characterized by single crystal x-ray diffraction. The DFT calculation results not only suggest that compound **1** possesses good stability, but also indicate that there is effective communication between inorganic [MoO$_4$]$^{2-}$ unit and metal-organic {Mn(salpn)(H$_2$O)}$^+$ moieties. Magnetic analysis studies disclosed that the [MoO$_4$]$^{2-}$ unit transmits very weak antiferromagnetic coupling within three [Mn(salpn)(H$_2$O)]$^+$ moieties. Our research, to some extent, provides a new path for the design and synthesis of hybrid materials between metal-Schiff base complexes and simple inorganic salts. Further research will focus on the reactions between different types of inorganic salts and metal-Schiff base complexes to obtain new classes of metal-Schiff base hybrids.

Author Contributions: Methodology, Q.W. and Y.X.; Investigation, Q.W., F.J., X.-D.X., T.L., and Y.L.; Resources J.-R.S.; Software, Conceptualization Q.W. and J.-C.X.; Formal analysis, Y.L. and J.-R.S.; Validation, J.-C.X. and T.L.; Supervision, Q.W.; Writing-original draft preparation, J.-C.X.; Project administration, Q.W.; Visualization, Q.W. and J.-C.X.; Writing-review and editing, J.-C.X.; Funding acquisition, Q.W.

References

1. Mirzaei, M.; Eshtiagh-Hosseini, H.; Alipour, M.; Frontera, A. Recent developments in the crystal engineering of diverse coordination modes (0–12) for Keggin-type polyoxometalates in hybrid inorganic–organic architectures. *Coordin. Chem. Rev.* **2014**, *275*, 1–18. [CrossRef]

2.   Miras, H.N.; Yan, J.; Long, D.-L.; Cronin, L. Engineering polyoxometalates with emergent properties. *Chem. Soc. Rev.* **2012**, *41*, 7403–7430. [CrossRef] [PubMed]

3.   Xiong, J.; Luo, T.; Zhang, J.; Li, X.-X.; Lv, S.-F.; Peng, J.-J.; Li, M.; Li, W.; Nakamura, T. Two Supramolecular Inorganic—Organic Hybrid Crystals Based on Keggin Polyoxometalates and Crown Ethers. *Crystals* **2018**, *8*, 17. [CrossRef]

4.   Sosa, J.D.; Bennett, T.F.; Nelms, K.J.; Liu, B.M.; Tovar, R.C.; Liu, Y. Metal–Organic Framework Hybrid Materials and Their Applications. *Crystals* **2018**, *8*, 325. [CrossRef]

5.   Gupta, K.C.; Sutar, A.K. Catalytic activities of Schiff base transition metal complexes. *Coordin. Chem. Rev.* **2008**, *252*, 1420–1450. [CrossRef]

6.   Miyasaka, H.; Saitoh, A.; Abe, S. Magnetic assemblies based on Mn(III) salen analogues. *Coord. Chem. Rev.* **2007**, *251*, 2622–2664. [CrossRef]

7.   Fu, Z.; Liao, H.; Xiong, D.; Zhang, Z.; Yan, J.; Yin, D. A highly-efficient and environmental-friendly method for the preparation of Mn(III)–Salen complexes encapsulated HMS by using microwave irradiation. *Microporous Mesoporous Mater.* **2007**, *106*, 298–303. [CrossRef]

8.   Watanabe, T.; Owada, S.H.; Kawakami, H.; Nagaoka, S.; Murakami, E.; Ishiuchi, A.; Enomoto, T.; Jinnouchi, Y.; Sakurai, J.; Tobe, N. Protective effects of MnM2Py4P and Mn-salen against small bowel ischemia/reperfusion injury in rats using an in vivo and an ex vivo electron paramagnetic resonance technique with a spin probe. *Transplant. Proc.* **2007**, *39*, 3002–3006. [CrossRef]

9.   Zhang, J.-J.; Day, C.S.; Lachgar, A. Self-assembly and solvent-mediated structural transformation of one-dimensional cluster-based coordination polymer. *CrystEngComm* **2011**, *13*, 133–137. [CrossRef]

10.   Donmez, A.; Coban, M.B.; Kara, H. Cyan-Blue Luminescence and Antiferromagnetic Coupling of CN-Bridged Tetranuclear Complex Based on Manganese(III) Schiff Base and Hexacyanoferrate(III). *J. Clust. Sci.* **2018**, *29*, 951–958. [CrossRef]

11.   Wang, T.T.; Bao, S.S.; Ren, M.; Cai, Z.S.; Zheng, Z.H.; Xu, Z.L.; Zheng, L.M. Assembly of {Mn$_2$(salen)$_2$}$^{2+}$ Dimers by Cyclic V 4 O 12 4− Clusters: A 3 D Compound with Open-Framework Structure Exhibiting Slow Magnetization Relaxation. *Chem. Asian J.* **2013**, *8*, 1772–1775. [CrossRef] [PubMed]

12.   Wu, Q.; Chen, W.L.; Liu, D.; Liang, C.; Li, Y.G.; Lin, S.W.; Wang, E. New class of organic-inorganic hybrid aggregates based on polyoxometalates and Metal-Schiff-base. *Dalton Trans.* **2011**, *40*, 56–61. [CrossRef] [PubMed]

13.   Yan, A.-X.; Tan, H.-Q.; Liu, D.; Zhang, Z.-M.; Wang, E.-B. Two organic–inorganic hybrid materials based on the penta-nuclear {MMn4} (M = W and Mo) heterometallic clusters and Schiff-base ligands. *Inorg. Chem. Commun.* **2013**, *29*, 49–52. [CrossRef]

14.   Wu, Q.; Liu, H.; Hu, X.; Lu, J.; Wang, H. A New 1-D Organic–Inorganic Hybrid Dimer Chain Complex Constructed by Manganese(III)-(Schiff-base) and [WO$_4$]$^{2−}$ Unit. *J. Clust. Sci.* **2015**, *26*, 1203–1213. [CrossRef]

15.   Suzuki, K.; Sato, R.; Mizuno, N. Reversible switching of single-molecule magnet behaviors by transformation of dinuclear dysprosium cores in polyoxometalates. *Chem. Sci.* **2013**, *4*, 596–600. [CrossRef]

16.   Wu, Q.; Li, Y.-G.; Wang, Y.-H.; Clérac, R.; Lu, Y.; Wang, E.-B. Polyoxometalate-based {MnIII$_2$}–Schiff base composite materials exhibiting single-molecule magnet behaviour. *Chem. Commun.* **2009**, 5743–5745. [CrossRef] [PubMed]

17.   Sawada, Y.; Kosaka, W.; Hayashi, Y.; Miyasaka, H. Coulombic aggregations of Mn III salen-type complexes and keggin-type polyoxometalates: Isolation of Mn 2 single-molecule magnets. *Inorg. Chem.* **2012**, *51*, 4824–4832. [CrossRef]

18.   Meng, X.; Wang, H.-N.; Wang, X.-L.; Yang, G.-S.; Wang, S.; Shao, K.-Z.; Su, Z.-M. Construction and property investigation of inorganic–organic hybrid materials based on metal–salens and Keggin polyoxometalates. *Inorg. Chim. Acta* **2012**, *390*, 135–142. [CrossRef]

19.   Meng, X.; Qin, C.; Wang, X.L.; Su, Z.M.; Li, B.; Yang, Q.H. Chiral salen-metal derivatives of polyoxometalates with asymmetric catalytic and photocatalytic activities. *Dalton Trans.* **2011**, *40*, 9964–9966. [CrossRef]

20.   Lin, S.; Wu, Q.; Tan, H.; Wang, E. A new organic–inorganic hybrid based on Mn–salen and decavanadate. *J. Coord. Chem.* **2011**, *64*, 3661–3669. [CrossRef]

21.   Shyu, H.L.; Wei, H.H.; Wang, Y. Structure and magnetic properties of dinuclear [Mn(III)(salen)(H$_2$O)]$_2$(ClO$_4$)$_2$ and polynuclear [Mn(III)(salen)(NO$_3$)]n. *Inorg. Chim. Acta* **1999**, *290*, 8–13. [CrossRef]

22.   Boudreaux, E.A.L.; Mulay, L.N. *Theory and Applications of Molecular Paramagnetism*; Boudreaux, E.A., Mulay, L.N., Eds.; Wiley-Interscience: New York, NY, USA, 1976; 510p.

23. Dolomanov, O.V.; Bourhis, L.J.; Gildea, R.J.; Howard, J.A.K.; Puschmann, H. OLEX2: A complete structure solution, refinement and analysis program. *J. Appl. Crystallogr.* **2010**, *42*, 339–341. [CrossRef]

24. Spek, A.L. PLATON SQUEEZE: A tool for the calculation of the disordered solvent contribution to the calculated structure factors. *Acta Crystallogr.* **2015**, *71*, 9–18.

25. Spek, A.L. Single-crystal structure validation with the program *PLATON*. *J. Appl. Cryst.* **2003**, *36*, 7–13. [CrossRef]

26. Cambridge Crystallographic Data Centre. Available online: https://www.ccdc.cam.ac.uk/ (accessed on 2 December 2019).

27. Brown, I.D.; Altermatt, D. Bond-valence parameters obtained from a systematic analysis of the Inorganic Crystal Structure Database. *Acta Crystallogr. Section B* **1985**, *41*, 244–247. [CrossRef]

28. Barbour, L.J. Crystal porosity and the burden of proof. *Chem Commun.* **2006**, *11*, 1163–1168. [CrossRef]

29. Frisch, M.J.; Trucks, G.W.; Schlegel, H.B.; Scuseria, G.E.; Robb, M.A.; Cheeseman, J.R.; Scalmani, G.; Barone, V.; Mennucci, B.; Petersson, G.A.; et al. *Gaussian 09*; Gaussian, Inc.: Wallingford, CT, USA, 2009.